Available online at www.sciencedirect.com
ScienceDirect
Ceramics International 37 (2011) 127–137
CERAMICS INTERNATIONAL
www.elsevier.com/locate/ceramint

High thermally stable Mg-substituted tricalcium phosphate *via* precipitation

Ilaria Cacciotti *, Alessandra Bianco

Department of Chemical Sciences and Technologies, INSTM Research Unit Tor Vergata, University of Rome Tor Vergata, via della Ricerca Scientifica, 00133 Rome, Italy

Received 12 February 2010; received in revised form 20 May 2010; accepted 24 July 2010
Available online 21 August 2010

Abstract

Tricalcium phosphates incorporating small amounts of Mg show attractive biological performances in terms of enhanced bone apposition, bone in-growth and cell-mediated degradation. A systematic investigation on Mg-stabilized β-TCP (β-tricalcium phosphate, β-$Ca_3(PO_4)_2$) is presented. Microstructure, composition and thermal behaviour were investigated by means of thermogravimetry and differential thermal analysis (TG-DTA), induced coupled plasma-atomic emission spectroscopy (ICP-AES), Fourier transform infrared spectroscopy (FT-IR), N_2 adsorption isotherms, X-ray diffraction (XRD and HT-XRD), and scanning electron microscopy (SEM). Pure and Mg-substituted tricalcium phosphate precursors consisted of calcium-deficient hydroxyapatite, the specific surface area being 128 m^2/g and 87 m^2/g, respectively. Tricalcium phosphate nanostructured powders were obtained by thermal treatment above 800 °C. The incorporation of Mg within the calcium phosphate lattice promoted the formation of the β-TCP phase at slightly lower temperature and resulted in the stabilization of the β-polymorph at high temperature (*i.e.* 1600 °C).

Keywords: A. Powders: chemical preparation; B. Microstructure; D. Apatite; E. Biomedical applications

1. Introduction

Synthetic tricalcium phosphate (TCP, $Ca_3(PO_4)_2$) and hydroxyapatite (HAp, $Ca_{10}(PO_4)_6(OH)_2$) are the most important calcium phosphate-based ceramics for the production of either dense and porous scaffolds for bone reconstruction [1]. In particular, the β-tricalcium phosphate (β-TCP) is one of the most attractive biomaterials for bone repair since it shows an excellent biological compatibility, osteoconductivity, and safety in living tissues [2–4]. Some Authors reported the presence of magnesium in calcified living tissue, suggesting that Mg^{2+} might improve the biocompatibility and bioactivity of TCP ceramics [5]. However, although β-TCP has reached acceptance in biomedical applications, it shows low mechanical strength and fracture toughness [6]. Moreover, the poor densification upon sintering below the β- to α-transformation temperature has remarkably limited its clinical applications. It has been shown that this transformation is accompanied by volume expansion and reduced shrinkage rate, preventing further densification of TCP [7–9].

In the last years, several Authors investigated the mechanical properties of β-TCP. Yoshida et al. suggested that the sinterability of β-TCP is enhanced by the substitution of mono-and divalent metal ions. It has been demonstrated that the substitution of either Mg^{2+} up to 9.6 mol% or monovalent cations effectively improved the mechanical strength of β-TCP, the bending strength being 160 MPa for β-TCP doped with 7.6 mol% Mg^{2+} [10]. Toriyama et al. [11] reported that the addition of MgO enhanced the bending strength of β-TCP up to 197 MPa. Moreover, the presence of Mg^{2+} ions within the TCP lattice can inhibit grain growth during the sintering process [12]. It is well known that the low temperature form of β-TCP phase is stabilized at higher temperature through the incorporation of metal ions in the Ca(V) site of the β-TCP lattice [13].

To our knowledge, studies focused on the synthesis of Mg-substituted tricalcium phosphate powders [13–20] are rarely reported. The proposed methodologies followed either the conventional solid-state process or precipitation routes [14]. The procedure *via* solid-state reaction usually involves the addition of magnesium oxide (MgO) aimed to stabilize the

* Corresponding author. Tel.: +39 0672594482; fax: +39 0672594328.
E-mail address: ilaria.cacciotti@uniroma2.it (I. Cacciotti).

0272-8842/$36.00
doi:10.1016/j.ceramint.2010.08.023

β-TCP phase up to 1500 °C and thus to enable β-TCP to sinter without undergoing phase transformations [10,13,15–22]. Ryu et al. showed that MgO-doped hydroxyapatite/TCP ceramics exhibited high density and significantly enhanced mechanical properties. However, compositional and microstructural inhomogeneties might arise associated to the presence of impurities and to unreacted MgO [18].

In this context, the main significance to follow an aqueous precipitation method relies on the availability of homogeneous mixtures, making this route an effective process to synthesise tricalcium phosphate powders suitable for further processing (*i.e.* granules, dense or porous bodies and coatings) [23]. Generally, the preparation of β-TCP through aqueous precipitation involves at first the precipitation of calcium-deficient apatite (CDHAp). Further calcination in the range 700–800 °C leads to the formation of the β-TCP phase, according to the following reaction:

$$Ca_9HPO_4(PO_4)_5(OH) \rightarrow 3Ca_3(PO_4)_2 + H_2O$$

Moreover, to our knowledge, pure and substituted tricalcium phosphate powders obtained by precipitation route have been rarely investigated [23]. In this framework, this study presented a systematic and complete investigation of pure and Mg-substituted tricalcium phosphate powders synthesised by a precipitation methodology. The proposed paper covers the overall ceramic process from powder synthesis to calcined powders providing useful information for further technological approaches.

The actual composition of samples was determined by means of induced coupled plasma-atomic emission spectroscopy (ICP-AES), the thermal behaviour was investigated by thermogravimetry and differential thermal analysis (TG-DTA), the specific surface area was measured by means of N_2 adsorption isotherms and the microstructure observed by scanning electron microscopy (SEM). Characteristic functional groups were evidenced by Fourier transform infrared spectroscopy (FT-IR). X-ray diffraction (XRD) and high-temperature X-ray diffraction (HT-XRD) were also recorded aimed to follow phase evolution, calculate cell parameters and estimate cristallinity degree.

2. Materials and methods

2.1. Synthesis of pure and Mg-substituted tricalcium phosphate precursors

Tricalcium phosphate and Mg-substituted tricalcium phosphate (Mg-TCP) precursors were synthesised in a double-walled jacket reactor at 40 °C under magnetic stirring. In the case of Mg-TCP precursor, it has been assumed that magnesium ions would substitute for the calcium site in the apatite lattice. Sample designation and nominal compositions of synthesised materials are summarised in Table 1. TCP precursor was obtained by adding drop-wise (3–4 drops/s) 250 ml of an 1.2 M aqueous solution of calcium nitrate tetrahydrate ($Ca(NO_3)_2{\cdot}4H_2O$, *Aldrich* 99.2%, MW 236.15) to a diammonium hydrogen phosphate ($(NH_4)_2HPO_4$, *Aldrich* 99.2%, MW 132.06) solution. The pH was continuously monitored and adjusted to 7 ± 0.1 by adding either a diluted solution of NH_4OH or a solution of HNO_3.

In the case of the Mg-TCP precursor (Mg content ~1 wt.%), magnesium nitrate hexahydrate ($Mg(NO_3)_2{\cdot}6H_2O$ (*Carlo Erba*, *101.5%*, MW 256.41) was also added to the calcium nitrate solution. According to Table 1, the nominal composition, in terms of (Ca + Mg)/P ratio, was maintained at 1.50.

Precipitates were aged in mother liquors at room temperature for 24 h, washed with NH_4OH aqueous solution, vacuum filtered and finally dried in oven at 60 °C (*as-dried* samples).

In order to obtain a single-phase β-TCP powder the *as-dried* calcium phosphate precursors were further thermally treated above 800 °C.

2.2. Characterisation of pure and Mg-substituted tricalcium phosphate precursors

Chemical analyses of precursors were performed by inductively coupled plasma-atomic emission spectroscopy (*AES-ICP*, *JobinYvon JV 24R*). Detection limits of ICP analysis were 0.2 ppb at 393.366 nm for Ca, 76 ppb at 214.914 nm for P and 1 ppb at 279.553 for Mg.

The thermal behaviour of *as-dried* samples was investigated by simultaneous thermogravimetry and differential thermal analysis (*TG-DTA, Netzsch STA 409*) in the following conditions: sample weight about 70 mg, heating rate 10 °C/min, peak temperature 1600 °C, air flow 80 cm^3/min.

The microstructural features of *as-dried* samples and calcined (temperature range 800–1100 °C) powders were studied by scanning electron microscopy (SEM, *CAMBRIDGE STEREOSCAN 360 and Leo Supra 35*).

Infrared spectra (Fourier transform infrared spectroscopy, *FTIR Perkin Elmer*) were recorded in the region 500–4000 cm^{-1} using KBr pellets (1%wt/wt), spectral resolution 4 cm^{-1}.

The specific surface area (SSA) of *as-dried* samples and powders heated at 800 °C was evaluated by N_2 adsorption (*Sorptomatic 1900*, *Carlo Erba Instruments*) using Brunauer–Emmett–Teller (BET) method. The linearized form of BET equation is expressed by:

$$\frac{p}{v(\rho_0 - \rho)} = \frac{1}{v_m c} + \frac{(c-1)}{v_m c}\frac{p}{p_0}$$

Table 1
Sample designation, nominal and actual composition of *as-dried* TCP and Mg-TCP precursors.

Sample	Formula	Nominal Ca/P (molar ratio)	Actual Ca/P (molar ratio)	Nominal (Ca + Mg)/P (molar ratio)	Actual (Ca + Mg)/P (molar ratio)
TCP	$Ca_3(PO_4)_2$	1.500	1.508	–	–
Mg-TCP	$Ca_{2.875}Mg_{0.125}(PO_4)_2$	1.438	1.432	1.500	1.462

where p/p_0 is the relative vapour pressure of the adsorbate, v is the volume of gas adsorbed, v_m is the volume of gas adsorbed in a monolayer and c is a constant related to the energy of adsorption. A linear regression of the left side of the BET equation and p/p_0 yields a slope and intercept from which c and v_m are obtained. The specific surface area is then calculated from v_m [24].

The particle size (D_{BET}) was also calculated by assuming the primary particles to be spherical:

$$D_{BET} = \frac{6}{\rho s}$$

where ρ is the theoretical density of the sample (3.156 g/cm^3 for *as-dried* precursors) and s is the SSA [25].

X-ray diffraction (XRD) (Philips X'Pert 1710) (Cu K_α radiation λ = 1.5405600 Å, 2θ 20–55°, step size 0.010°, time per step 2 s, scan speed 0.005°/s) analyses were performed on both *as-dried* and calcined powders at different temperatures up to 1600 °C. Phase evolution of *as-dried* powders was followed by high-temperature XRD measurements (HT-XRD) (*Anton Paar HTK 1200*) in the following conditions: Cu K_α radiation λ = 1.5405600 Å, 2θ 20–55°, heating rate 5 °C/min, peak temperature 1100 °C, step size 0.010°, time per step 2 s, scan speed 0.005°/s.

According to Landi et al. [26], the crystallinity degree of *as-dried* samples (X_c), corresponding to the fraction of crystalline phase present in the examined volume, was evaluated by the relation:

$$X_c \approx 1 - \frac{V_{112/300}}{I_{300}}$$

where I_{300} is the intensity of (3 0 0) reflection of apatite structure and $V_{112/300}$ is the difference between the intensity of the (1 1 2) and (3 0 0) reflections.

The average crystallite size $D_{(hkl)}$ in nm was estimated following Debey–Scherrer equation [27]:

$$D_{(hkl)} = \frac{K\lambda}{\sqrt{\varpi^2 - \varpi_0^2}\cos\vartheta}$$

where K is the shape factor equal to 0.9, λ is the X-rays wavelength (equal to 1.541 Å for Cu K_α radiation), Θ is the Bragg's diffraction angle (in degrees) and ω is the full width at half maximum (FWHM). The diffraction peak at 25.8° (2Θ) corresponding to (0 0 2) Miller plane family of apatite lattice (JCPDS file #09-0432), and the diffraction peak at 32.9° (2Θ) corresponding to (3 0 0) Miller plane family, were chosen to calculate the average crystal size along to the crystallographic axis c and a, respectively, ω_0 corresponds to the instrumental width (0.087) [28]. The length of coherent domains $D_{(2010)}$ in TCP crystallites was also calculated using the line broadening of the (2 0 1 0) peak (diffraction angle 2Θ (31.0°)) [20], applying the Scherrer's equation to XRD spectra of samples calcined at 800 °C.

Cell parameters of the tricalcium phosphate phase were estimated through the algorithm *TREOR* (*Philips X'Pert Plus software*), using XRD diffraction patterns of samples calcined at 1100 °C, the reference for tricalcium phosphate being JCPDS #09-0169 (a = 10.432(3) Å, b = 10.432(3) Å, c = 37.39 Å, space group $R3c$ (167), theoretical density 3.072 g/cm^3, V = 3520.91 Å^3, Z = 21).

3. Results and discussion

3.1. Composition of TCP and Mg-TCP precursors

In Table 1 the actual and nominal compositions of the *as-dried* samples are compared. The actual composition of TCP and Mg-TCP precursors in terms of Ca/P molar ratio was very close to the expected stoichiometric value. These results suggest that the proposed methodology allows a strict control over the sample composition. However, in the case of Mg-TCP precursor, the loss of magnesium resulted in a lower (Ca + Mg)/P molar ratio with respect to the nominal value, the actual Mg content being reduced from 2.50 mol% (0.99 wt.%) to 1.47 mol% (0.58 wt.%).

3.2. Microstructure and specific surface area of as-dried and calcined TCP and Mg-TCP precursors

The morphology of pure and Mg-substituted *as-dried* and calcined (at 800 °C and 1100 °C) samples was determined by SEM observations, in order to evidence the influence of Mg incorporation and the calcination temperature on particles morphology and size (Fig. 1a–f).

In Fig. 1a and b SEM micrographs of *as-dried* pure and Mg-substituted samples are reported. In good agreement with the literature [15,29–31], *as-dried* samples consisted of submicrometric flake-like agglomerates. Calcination of *as-dried* samples at 800 °C produced nanoparticles of uniform size (Fig. 1c and d). As shown in Fig. 1e and f, further thermal treatment at 1100 °C induced remarkable grain coarsening and micro-sized particles were obtained [32,33]. Besides, in the case of Mg-TCP, extensive sintering was also observed (Fig. 1f). In agreement with Ref. [10], the presence of divalent substitution cations induces the enhancement of tricalcium phosphate sinterability.

Results of SSA are reported in Table 2. It resulted that *as-dried* TCP precursor showed a remarkable higher SSA with respect to the Mg-substituted one, the value being 128 m^2/g and 87 m^2/g, respectively.

As expected, the SSA of samples calcined at 800 °C (14 m^2/g and 4 m^2/g for pure and Mg-substituted powders, respectively) was significantly reduced with respect to *as-dried* ones, due to diffusion controlled smoothening of the particles surfaces [20].

Table 2
Specific surface area (SSA) and average particle size (D_{BET}) of pure tricalcium phosphate (TCP) and Mg-substituted tricalcium phosphate (Mg-TCP) precursors *as-dried* and calcined at 800 °C.

Sample	*As-dried*[a] (m^2/g)	Calcined (m^2/g)	D_{BET}[b] (nm)
TCP	128	14	15
Mg-TCP	87	4	22

[a] Samples were preliminarily treated with EtOH in order to eliminate absorbed water.
[b] The average particle size (D_{BET}) referred to the *as-dried* precursors.

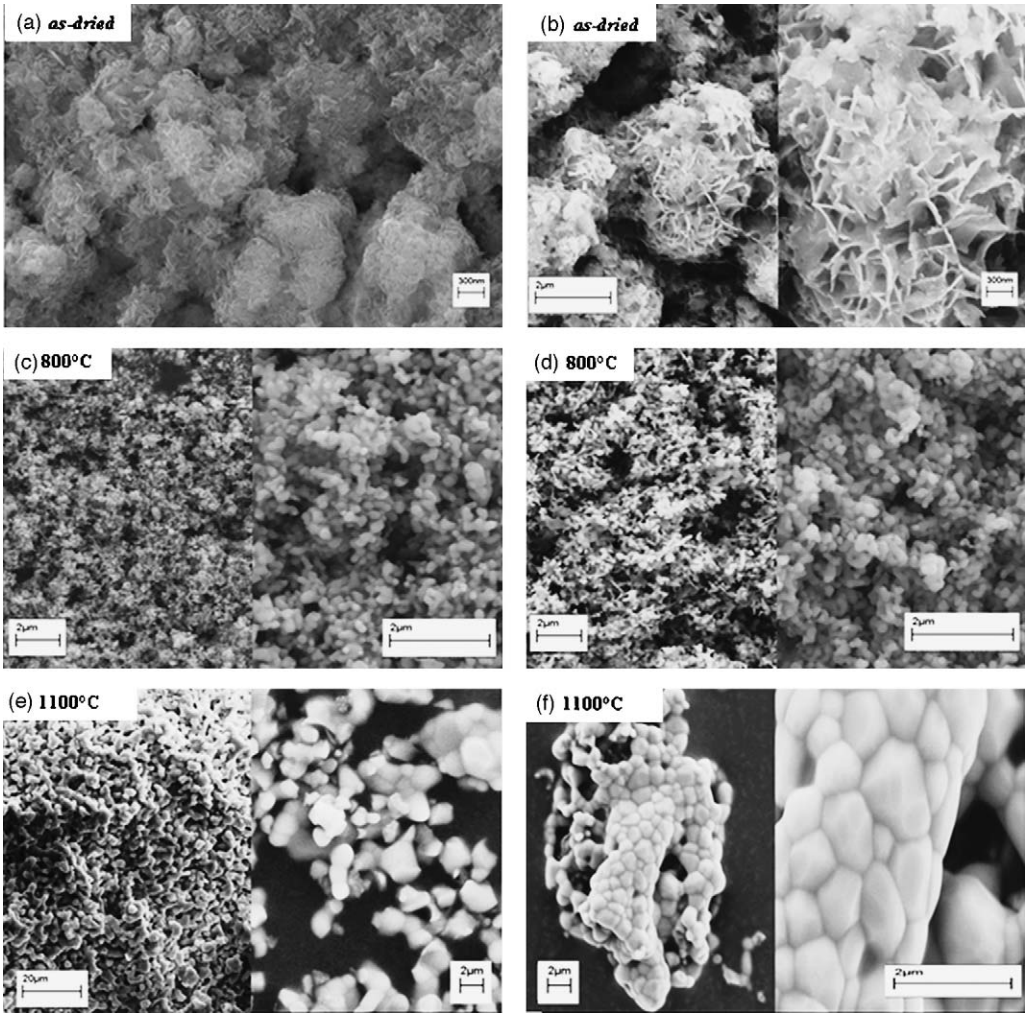

Fig. 1. SEM micrographs of *as-dried* precursors (a and b), TCP and Mg-TCP powders calcined at 800 °C (c and d), and TCP and Mg-TCP powders calcined at 1100 °C (e and f).

The average particle size (D_{BET}) of *as-dried* samples was calculated as about 15 nm and 22 nm for the TCP and the Mg-TCP precursors, respectively. These results were in good agreement with SEM observations reported in Fig. 1a and b.

3.3. Phase analysis, crystallinity, and crystallite size of as-dried TCP and Mg-TCP precursors

XRD spectra of TCP and Mg-TCP precursors are compared in Fig. 2. Both samples showed the typical diffraction pattern of the calcium-deficient hydroxyapatite (CDHAp) [1,14]; the crystallinity degree was around 20% for both samples, in good agreement with the Literature [34–36].

Moreover, according to [14,34,37], the XRD spectrum of the Mg-TCP precursor clearly evidenced merged reflections in the 2θ ranges 28–32° and 45–55°. This feature suggested that Mg incorporation within apatite lattice induced increased reticular defects.

Moreover, the mean crystallite size was also evaluated. In the case of the TCP precursor it was about 17 nm along the *c* axis and 8 nm along the *a* axis. For Mg-TCP precursor, the mean crystallite size was about 14 nm along *c* axis and 4 nm along the *a* axis [38].

3.4. Thermal stability of TCP and Mg-TCP precursors

Phase evolution was followed and the thermal decomposition temperature accurately defined by HT-XRD (Fig. 3a and b). The β-TCP (β-tricalcium phosphate, β-$Ca_3(PO_4)_2$, JCPDS #09-0169) diffraction peaks appeared at about 680 °C and 620 °C for the TCP and Mg-TCP precursors, respectively, together with the progressive decreasing of the broad reflections associated to the calcium-deficient hydroxyapatite (CDHAp). The transformation of precursors in the beta tricalcium phosphate (β-TCP) phase was completed around 800 °C and 740 °C for pure and Mg-substituted samples, respectively. According to [23,35], the presence of Mg^{2+} thus promoted the formation of the β-TCP phase. In more details, the presence of magnesium within the calcium phosphate lattice induced the CDHAp → TCP transformation to occur at slightly lower temperatures, the mechanism being more efficient with increasing the Mg content [15,39]. This effect

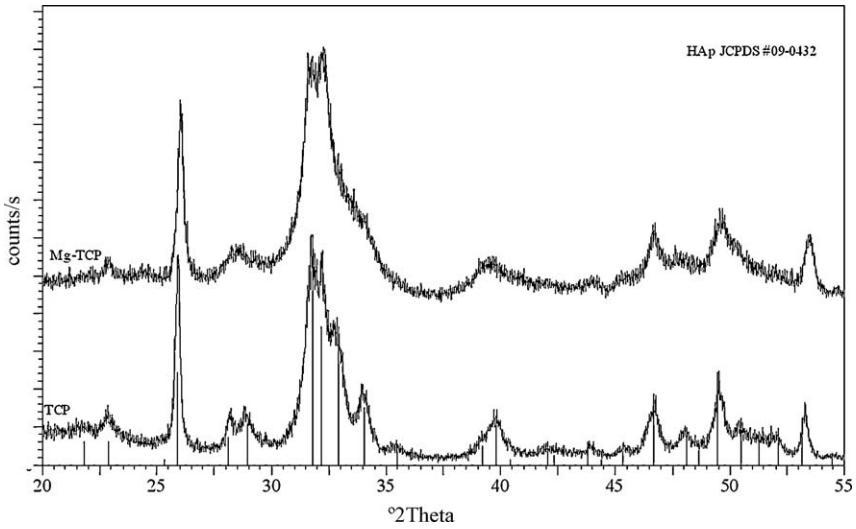

Fig. 2. XRD patterns of *as-dried* TCP and Mg-TCP precursors.

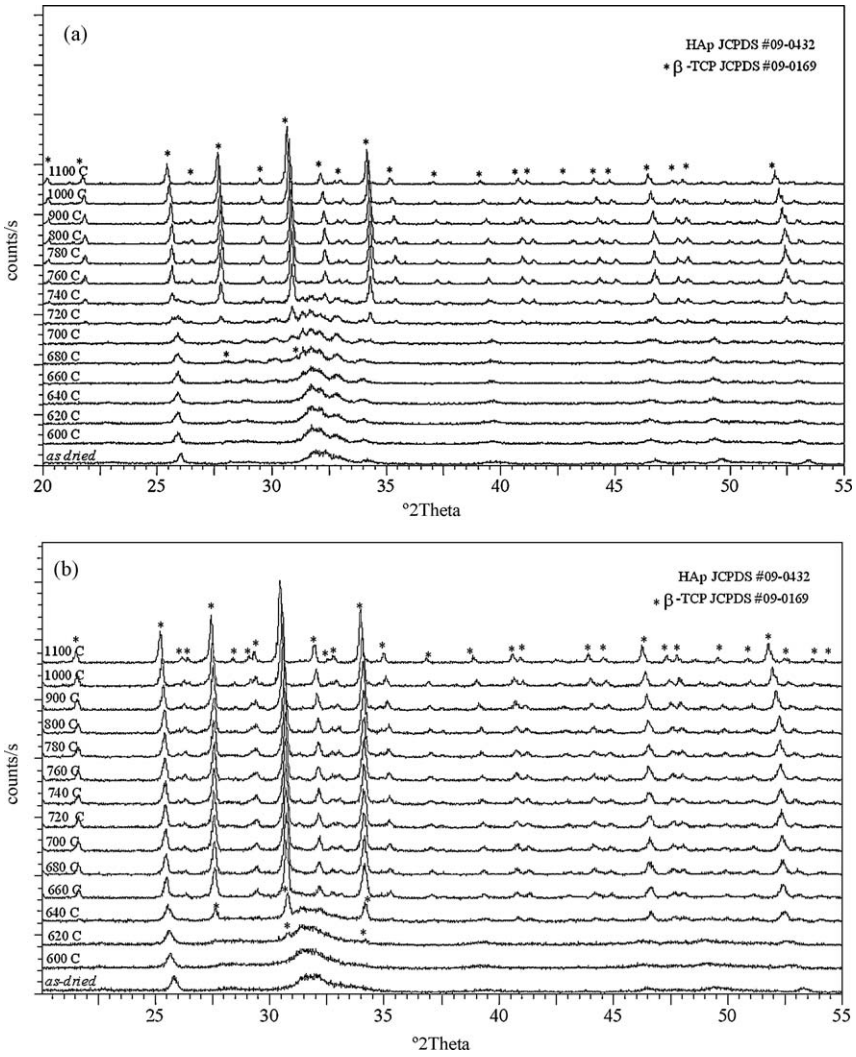

Fig. 3. (a) HT-XRD spectra of the TCP precursor, temperature range 30–1100 °C. (b) HT-XRD spectra of the Mg-TCP precursor, temperature range 30–1100 °C.

was attributed to the destabilizing effect of Mg imputable to the small ionic radius of Mg^{2+} (0.65 Å) with respect to Ca^{2+} (0.99 Å) [40].

It is important to underline that TCP cannot be synthesized directly in aqueous solution by wet method. The precipitate is an apatitic tricalcium phosphate ($Ca_9(HPO_4)(PO_4)_5(OH)$), consisting of calcium-deficient hydroxyapatite (CDHAp), $Ca_{10}(PO_4)_6(OH)_2$ where HPO_4^{2-} ion partially substitutes the PO_4^{3-} groups. The crystallization of anhydrous β-TCP requires further calcination of the apatitic compound at temperatures over 750 °C [15]. Non-stoichiometric apatites $Ca_{10-x}(HPO_4)_x(PO_4)_{6-x}(OH)_{2-x}$ with $0 \leq x \leq 1$ can be precipitated, the value of x depending on the synthesis conditions. The most important parameters to control are the pH and the temperature. Though the values reported in the Literature are scattered, the pH value is rather maintained at a value close to the neutrality, slightly acid, and low temperatures are generally used. The kinetics of formation of the precipitates is still misunderstood [15,41].

A specific difficulty linked with non-stoichiometric apatite synthesis is the high variability of the powder composition after calcination even for very low variations of the Ca/P molar ratio of the initial precipitate [15]. Some Authors observed that pure TCP is usually formed by calcination of a powder with Ca/P equal to 1.500, while for Ca/P values higher than 1.500 HAp is formed as a second phase. In the case of powders with Ca/P values lower than 1.500 calcium pyrophosphate (CPP, $Ca_2P_2O_7$) might appear as second phase. According to Destainville et al. [15], the evolution of the chemical composition of precipitates with Ca/P <1.500 can support two hypotheses. On the basis of the first one, it can be supposed that for powders with Ca/P molar ratio <1.5, the precipitation begins from dicalcium phosphate dihydrate (DCPD, $CaHPO_4{\cdot}2H_2O$) formation, followed by its slow and partial hydrolysis into apatitic tricalcium phosphate, the final mixture containing dicalcium phosphate anhydrous (DCPA, $CaHPO_4$) as a second phase after drying [14,42]. The second hypothesis is concerned with the precipitation process of a single-phase non-stoichiometric apatite [43]. The first step is the precipitation of an amorphous compound ($Ca_9(PO_4)_6$, nH_2O), its stoichiometry being very close to that of TCP. This step is followed by the hydrolysis of phosphate groups (PO_4^{3-}) into hydrogenophosphate (HPO_4^{2-}) and hydroxide ions (OH^-). Finally, these reactions lead to a non-stoichiometric compound of apatite structure ($Ca_9(HPO_4)_x(PO_4)_{6-x}(OH)_x$).

Furthermore, in the case of TCP, the formation of the α-TCP (α-$Ca_3(PO_4)_2$, JCPDS #09-0348) polymorph was observed at about 1200 °C (Fig. 4), accordingly with the phase diagram. In fact, on the basis of the phase diagram, the β-polymorph of TCP is usually the stable phase up to 1125 °C, at higher temperature the transition to the α-polymorph occurs, being the stable phase up to 1430 °C [14,44]. It has been demonstrated that this phase transition temperature can be influenced either by synthesis parameters or by the presence of substituting ions, including Mg^{2+} [14]. The role of Mg in stabilizing the β-TCP phase can be represented by the following reaction [23]:

$$Ca_9Mg_x(HPO_4)(PO_4)_5(OH) \rightarrow 3(Ca_{3-(x/3)}Mg_{x/3})(PO_4)_2 + H_2O$$

where x is the content of Mg.

In good conformity with these considerations, in the case of the Mg-TCP sample, the incorporation of Mg within the apatite lattice resulted in the stabilization of the β-TCP polymorph at higher temperatures, *i.e.* up to 1600 °C (Fig. 4). This result was supported by Literature data, the transition temperature of Mg-substituted TCP (8 mol%) increasing up to 1540 °C [13,23,45].

In addition, it resulted that the incorporation of Mg^{2+} into the TCP lattice produced a shift of diffraction peaks toward higher 2Θ values due to the contraction of lattice parameters, associated again to the different size of the two cations (Tables 3 and 4).

In Table 3, 2Θ and d-spacing values relative to the maximum intensity plane (0 2 1 0) of β-TCP of both samples are reported, in good agreement with Literature data [20] and with the values reported in the JCPDS files (JCPDS # 09-0169 for TCP and JCPDS #70-0681 for Mg-substituted TCP ($Ca_{2.86}Mg_{0.14}(PO_4)_2$), Mg 1.1 wt.%).

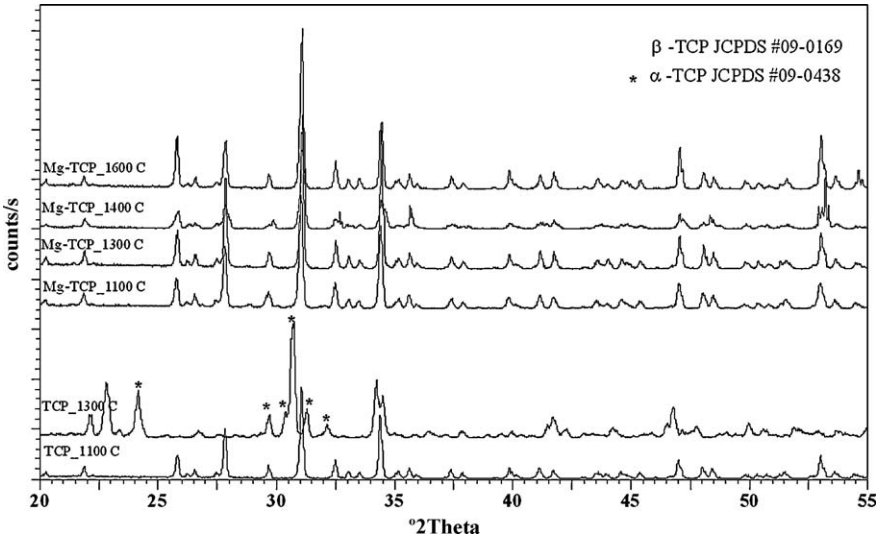

Fig. 4. XRD spectra of the TCP precursor calcined at 1100 °C and 1300 °C and of the Mg-TCP precursor calcined at 1100 °C, 1300 °C, 1400 °C and 1600 °C.

Table 3
Diffraction angles (2θ) and d-spacing values derived from experimental XRD patterns of TCP and Mg-TCP precursors calcined at 800 °C (β-TCP and β-Mg-TCP).

Sample	(0 2 1 0)	
	d-Spacing (Å)	2Θ
β-TCP	2.8791	31.037
β-Mg-TCP	2.8741	31.092

Table 4
Calculated cell parameters of β-tricalcium phosphate (β-TCP) and β-Mg-substituted tricalcium phosphate substituted (β-Mg-TCP) calcined at 800 °C.

Sample	a (Å)	b (Å)	c (Å)	V (10^6 pm^3)
β-TCP	10.443(5)	10.443(5)	37.393(8)	3531.432
β-Mg-TCP	10.425(8)	10.425(8)	37.40(2)	3519.370

These results showed that the 2Θ and d-spacing of Mg-TCP were shifted with respect to TCP, thus confirming once more the stabilization of the β-TCP phase induced by the presence of Mg.

Calculated cell parameters are reported in Table 4. In good agreement with the Literature [34,36,37,46,47], a reduction of a and b was detected and it can be associated to the contraction of the unit cell. Once again this is the result of different ionic radius between Mg^{2+} (0.65 Å) and Ca^{2+} (0.99 Å) [23].

Finally, the mean crystallite size of TCP and Mg-TCP precursors calcined at 1100 °C (*i.e.* beta tricalcium phosphate and Mg-substituted beta tricalcium phosphate) was estimated as about 11.5 nm and 6 nm, respectively [38].

3.5. Thermal behaviour of TCP and Mg-TCP precursors

Aimed to further evidence the influence of magnesium substitution on the phase transformation, simultaneous thermogravimetry and differential thermal analyses were performed.

In details, TG curves of *as-dried* TCP and Mg-TCP precursors showed two weight distinct losses [48] (Fig. 5). The first occurred in the range 20–700 °C, the loss was about 37 wt.% and 17 wt.% for TCP and Mg-TCP precursors, respectively. This first step has been ascribed to the loss of adsorbed water accompanied by the dehydration of HPO_4^{2-} ions into pyrophosphate ions, according to the mechanism proposed by Mortier et al. [15,49,50] for calcium-deficient hydroxyapatite (CDHAp):

$$Ca_{10-x}(HPO_4)_{2x}(PO_4)_{6-2x}(OH)_2 \rightarrow Ca_{10-x}(P_2O_7)_{x-z}(PO_4)_{6-2x+2z}(OH)_{2(1-z)} + (x+z)H_2O$$

The second loss of about 0.5–0.7% occurred between 700 °C and 800 °C and might be attributed to the reaction between OH ions of apatite and the pyrophosphate ions formed at lower temperature with consequent loss of water, as reported in the following equation:

$$P_2O_7^{4-} + OH^- \rightarrow 2PO_4^{3-} + H_2O$$

This process led to the decomposition of the apatitic phase into β-TCP [15,32,50], as demonstrated by the presence of an endothermic peak around 750–800 °C in the DTA patterns (Fig. 5). The overall removal of water around 750 °C coincides with the beginning of an endothermic transformation corre-

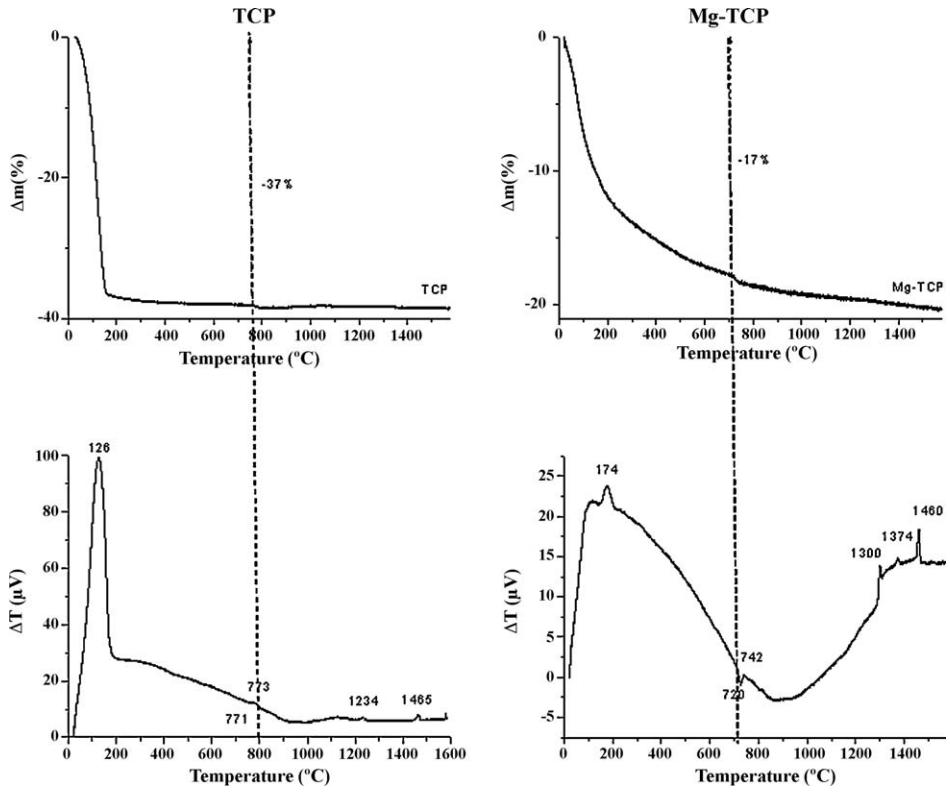

Fig. 5. TG-DTA patterns of *as-dried* TCP and Mg-TCP precursors.

sponding to the crystallisation of β-$Ca_3(PO_4)_2$ from the amorphous state [50].

Moreover, the endothermic peak in the DTA patterns associated to the decomposition of the apatitic phase into β-TCP was shifted to lower temperatures for Mg-substituted sample (*i.e.* from 773 °C to 742 °C) (Fig. 5) [15,32], supporting the XRD results (Fig. 3a and b). In fact, the CDHAp → TCP transformation is a multi step process, the first exothermic reaction being immediately followed by an endothermic step corresponding to the dehydroxylation of CDHAp that finally leads to the β-TCP phase. This transformation occurred at temperatures between 700 °C and 800 °C for both powders, although the presence of magnesium in the calcium phosphate lattice altered the transformation from CDHAp to TCP to slightly lower temperatures. Indeed, also the exothermic peak resulted shifted from 771 °C for TCP precursor to 720 °C for the Mg-TCP one, in the DTA patterns (Fig. 5). These findings were in good agreement with Marchi et al. [20].

Besides, DTA analyses (Fig. 5) evidenced the peaks associated to the β-TCP → α-TCP phase transition and to the high-temperature α-TCP → α′-TCP transformation. The DTA curve of the TCP precursor showed a first endothermic peak at around 1234 °C, associable with the transformation β → α. A shift of about 50 °C of the β → α transformation temperature (*i.e.* from 1180 °C to 1230 °C) with respect to the phase diagram was also reported in Ref. [20]. Moreover, a second endothermic peak around 1465 °C assigned to the α → α′ allotropic transformation was detected, in agreement with the phase diagram [14,15].

Finally, the DTA curve of the Mg-TCP precursor showed several endothermic peaks in the range 1300–1460 °C (Fig. 5). According to Malysheva et al., the presence of several endothermic effects is evidence of the multistage dehydration and of the coordination bond between water and the Ca^{2+} ion, since otherwise water would be removed in a single step. The first removed water molecules are those bonded in the crystal lattice with the PO_4^{3-} anion by weak hydrogen bonds or with the Ca^{2+} cation by coordination bonds. Next, H_2O molecules incorporated in the first coordination sphere of calcium are removed [50].

The peak observed at a temperature of about 1300 °C, associated with a much stronger endothermic effect than the allotropic transformations, could be related to the formation of an eutectic melt (liquid phase) between α-$Ca_2P_2O_7$ and $Ca_3(PO_4)_2$, according to the phase diagram CaO–P_2O_5 proposed by Kreidler and Hummel [15,51]:

$$\alpha\text{-}Ca_3(PO_4)_2 + \alpha\text{-}Ca_2P_2O_7 \rightarrow \alpha\text{-}Ca_3(PO_4)_2 + \text{liquid}(1280-1290\,^{\circ}C)$$

According to Destainville et al. [15], this peak can be detected in calcium phosphate powders containing more than 0.5 wt.% $Ca_2P_2O_7$, suggesting that the obtained β-TCP powder might contain $Ca_2P_2O_7$ as second phase. It is possible that this phase, together with the magnesium addition, alters the β → α phase transformation temperature.

Therefore, DTA is very efficient for the detection of very low amounts of CPP [15], being very difficult to identify this phase by XRD analysis. In fact, the main diffraction peak of β-$Ca_2P_2O_7$ at 2θ 29.551 is superposed with the diffraction peak of the β-TCP phase corresponding to (3 0 0) Miller plane family (JCPDS #09-0169).

Besides, the DTA curve presented two further sharp peaks at 1374 °C and 1460 °C. The first peak might be attributed to the melting of pyrophosphate ($Ca_2P_2O_7$, JCPDS #09-0345), resulting from the condensation reaction of the residual $CaHPO_4$, and the latter to the decomposition of unreacted HAp [52].

3.6. FT-IR analysis of as-dried and calcined TCP and Mg-TCP precursors

In Fig. 6a and b FT-IR spectra of *as-dried* TCP and Mg-TCP precursors are reported. Both *as-dried* sample presented the characteristic pattern of calcium-deficient hydroxyapatite [53,54]: ν OH (3568 cm^{-1}) and δ OH (633 cm^{-1}); ν_1 PO_4 (962 cm^{-1}), ν_3 PO_4 (broad band 1020–1120 cm^{-1}) and ν_4 PO_4 (562 cm^{-1} and 602 cm^{-1}); ν_2 CO_3 (875 cm^{-1}). The weak absorption peak at 875 cm^{-1} could be ascribed to the P–O–H vibration in the HPO_4^{2-} group typical of non-stoichiometric HAps [40]. The broad band at 2500–3700 cm^{-1} and the sharp peak at 1636 cm^{-1} were associated to the presence of either combined or absorbed water. Moreover, the lack of bands in the range 700–750 cm^{-1} indicated the absence of calcium carbonates, *i.e.* calcite (712 cm^{-1}), aragonite (713 cm^{-1} and 700 cm^{-1}) and valerite (745 cm^{-1}). Finally, the absorption band at 1385 cm^{-1} ascribed to nitrates was absent, indicating that washings were efficient. Furthermore, the Mg-TCP precursor showed a decreased intensity of OH^{-1} vibration modes at 633 cm^{-1} (Fig. 6a) and 3568 cm^{-1} (Fig. 6b), as well as a considerable broadening of the 700–1700 cm^{-1} PO_4^{3-} bands [35,36,55]. These effects are typical for Mg-substituted calcium phosphates synthesized by wet methods and have to be associated with the increased lattice disorder due to HPO_4^{2-} substitution [35,37,56].

As expected, FT-IR spectra of TCP and Mg-TCP precursors calcined at 800 °C and 1100 °C differed considerably from those recorded for the *as-dried* materials (Fig. 6c and d). In details, the intensity of peaks associated to H_2O was remarkably decreased, and, with increasing the calcination temperatures, the PO_4^{3-} vibration peaks at 603 cm^{-1} and 568 cm^{-1} gradually merged [32].

In particular, the Mg-TCP precursor calcined at 800 °C showed the typical FT-IR spectrum of the tricalcium phosphate: the peaks at about 756 cm^{-1} and 1212 cm^{-1} might be ascribed to the symmetrical stretching vibration of the P–O–P group of the pyrophosphates (Fig. 6d). These bands were not detected in the spectrum of the TCP precursor calcined at 800 °C, suggesting that the investigated sample did not contain this compound (Fig. 6c).

In fact, according to Raynaud et al. [17], in the case of apatites with Ca/P ratio <1.50, bands ascribable to pyrophosphates at 720–725 cm^{-1}, 920 cm^{-1} and 1200 cm^{-1} might be detected [57]. On the other side, in calcium phosphates with Ca/P ratio equal to 1.50, the bands associated to pyrophosphates are absent. This phenomenon agrees with the condensation of

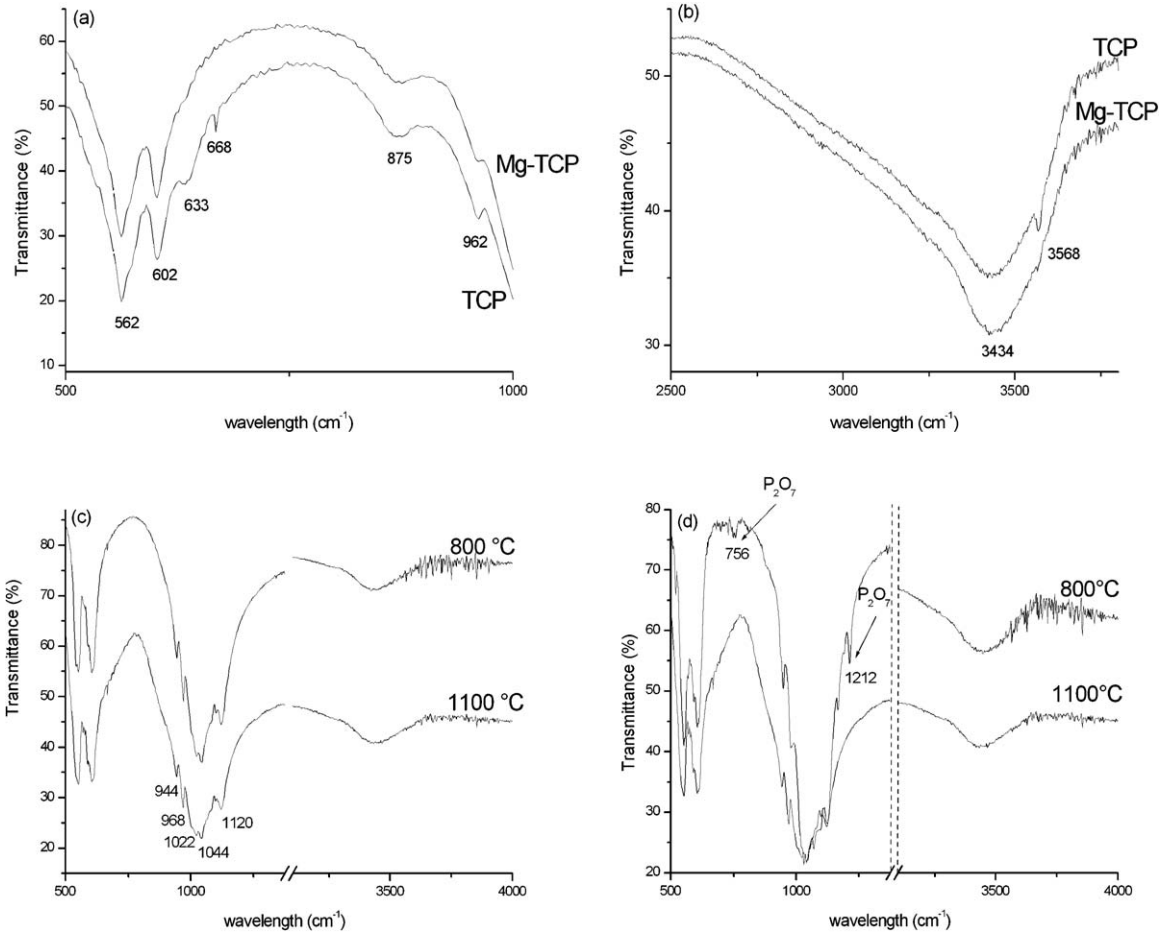

Fig. 6. FT-IR spectra of: (a) *as-dried* TCP and Mg-TCP precursors betweeen 500 cm^{-1} and 1000 cm^{-1}; (b) *as-dried* TCP and Mg-TCP precursors betweeen 2500 cm^{-1} and 4000 cm^{-1}; (c) TCP precursor calcined at 800 °C and 1100 °C; (d) Mg-TCP precursor calcined at 800 °C and 1100 °C.

hydrogenophosphate groups in calcium-deficient apatite. It could be ascribed to the conversion of $CaHPO_4$ into β-$Ca_2P_2O_7$, that occurs in the range 450–850 °C, according to the mechanism proposed by Mortier et al. [49]. This reaction was followed by the dehydroxylation of apatitic TCP into β-$Ca_3(PO_4)_2$ above 700 °C [17,50]:

$$2CaHPO_4 \xrightarrow{450\,^{\circ}C} \delta Ca_2P_2O_7 + H_2O$$

$$\delta Ca_2P_2O_7 \xrightarrow{850\,^{\circ}C} \beta\text{-}Ca_2P_2O_7$$

This corresponds with the decomposition of calcium-deficient HAp that occurs around 750 °C, according to the overall reaction:

$$Ca_{10-x}(HPO_4)_x(PO_4)_{6-x}(OH)_{2-x} \rightarrow (1-x)Ca_{10}(PO_4)_6(OH)_2 + 3xCa_3(PO_4)_2 + xH_2O$$

The pyrophosphates characteristic bands disappear in the case of sample thermally treated at temperature higher than 1000 °C, as observed in the case of Mg-TCP precursor calcined at 1100 °C (Fig. 6d). Moreover, the TCP precursor heated at 1100 °C showed the characteristic peaks of β-TCP (Fig. 6c) [15,32], in good agreement with the previous discussed results. In details, the peaks associated to the PO_4^{3-} were detected at 944 cm^{-1}, 968 cm^{-1}, 1044 cm^{-1}, 1094 cm^{-1}, 1120 cm^{-1} [58] accompanied by the disappearance of vibrations related to the P–O–P group and of the bands of the hydroxyl group. This behaviour could be ascribed to the reaction occurring between the $P_2O_7^{2-}$ and OH^-, which usually takes place in the temperature range 500–680 °C [50]:

$$P_2O_7^{2-} + 2OH^- \rightarrow 2PO_4^{3-} + H_2O$$

4. Conclusions

The synthesis of pure and Mg-substituted β-TCP powders was successfully pursued *via* a precipitation route, starting from $Ca(NO_3)_2{\cdot}4H_2O$ and $(NH_4)_2HPO_4$, followed by a thermal treatment above 800 °C. In the case of Mg-substituted powder, $Mg(NO_3)_2{\cdot}6H_2O$ was added as magnesium source. TCP and Mg-TCP precursors consisted of submicrometric flake-like agglomerates. The specific surface area was 128 m^2/g and 87 m^2/g for the TCP and Mg-substitute TCP *as-dried* precursors, respectively. Calcination of *as-dried* samples at 800 °C produced nanoparticles of uniform size with a significantly reduced specific surface area (4–14 m^2/g). Further thermal treatment at 1100 °C induced remarkable grain coarsening and micro-sized particles were obtained. Moreover, in the case of Mg-TCP, extensive sintering was also observed. On the basis of a widespread characterisation, nanosized single-phase β-TCP

powders were obtained by thermal treatment at 800 °C. The incorporation of Mg promoted the formation of the β-TCP phase and resulted in the stabilization of the β-polymorph up to 1600 °C.

Acknowledgments

This work was supported by PRIN 2006-2008 project titled "*Design and production of organic, inorganic and hybrid nanostructured scaffolds as substrates for the differentiation of stem cells in regenerative medicine*".

The Authors wish to acknowledge Dr. C. Bellitto and Dr. E. Bauer (ISM, CNR-Montelibretti, Rome, Italy) for FT-IR facilities and Dr. F. Nanni (University of Rome Tor Vergata) for SEM analyses.

References

[1] M. Jarcho, Calcium phosphate ceramics as hard tissue prosthetics, Clin. Orthop. Relat. Res. 157 (259) (1981).
[2] S. Kotani, Y. Fujita, T. Kitsugi, T. Nakamura, T. Yamamuro, C. Ohtsuki, T. Kokubo, Bone bonding mechanism of β-tricalcium phosphate, J. Biomed. Mater. Res. 25 (1991) 1303–1315.
[3] L.L. Hench, J. Wilson, An Introduction to Bioceramics, World Scientific, London, U.K., 1993.
[4] H. Yonezaki, T. Hayashi, T. Nakagawa, H. Kurosawa, K. Shibuya, K. Ioku, Influence of surface microstructure on the reaction of the active ceramics in vivo, J. Mater. Sci.: Mater. Med. 9 (1998) 381–384.
[5] K. de Groot, Bioceramics of Calcium Phosphate, CRC Press, Boca Raton, FL, 1983.
[6] F.-H. Lin, C.-J. Liao, K.-S. Chen, J.-S. Sun, C.-P. Lin, Petal-like apatite formed on the surface of tricalcium phosphate ceramic after soaking in distilled water, Biomaterials 22 (12) (2001) 2981–2992.
[7] H.-S. Ryu, H.-J. Youn, K.-S. Hong, B.-S. Chang, C.-K. Lee, S.-S. Chung, An improvement in sintering property of beta-tricalcium phosphate by addition of calcium pyrophosphate, Biomaterials 23 (2002) 909–914.
[8] R. Famery, P.B. Richard, Preparation of α- and β-TCP ceramics, with and without magnesium addition, Ceram. Int. 20 (1994) 327–336.
[9] K. Itatani, T. Nishioka, S. Seike, F.S. Howell, A. Kishioka, M. Kinishita, Sinterability of β-orthophosphate powder prepared by spray pyrolysis, J. Am. Ceram. Soc. 77 (1994) 801–805.
[10] K. Yoshida, W.N. Kondo, H. Kita, Effect of substitutional monovalent and divalent metal ions on mechanical properties of β-tricalcium phosphate, J. Am. Ceram. Soc. 88 (2005) 2315–2318.
[11] M. Toriyama, S. Kawamura, H. Nagae, K. Ishida, Effect of MgO addition on bending strength of sintered β-tricalcium phosphate prepared by mechanochemical synthesis, J. Ceram. Soc. Jpn. (Yogyo-Kyokai-Shi) 95 (1987) 822–824 (in Japanese).
[12] K. Itatani, M. Takahashi, F.S. Howell, M. Aizawa, Effect of metal-oxide addition on the sintering of β-calcium orthophosphate, J. Mater. Sci.: Mater. Med. 13 (2002) 707–713.
[13] R. Enderle, F. Gotz-Neunhoeffer, M. Gobbels, F.A. Muller, P. Greil, Influence of magnesium doping on the phase transformation temperature of β-TCP ceramics examined by Rietveld refinement, Biomaterials 26 (2005) 3379–3384.
[14] J.C. Elliott, Structure and Chemistry of the Apatites and Other Calcium Orthophosphates. Studies in Inorganic Chemistry, vol. 18, Elsevier, Amsterdam, 1994.
[15] A. Destainville, E. Champio, D. Bernache-Assollant, E. La Borde, Synthesis, characterization and thermal behaviour of apatitic tricalcium phosphate, Mater. Chem. Phys. 80 (2003) 269–277.
[16] S.N. Radin, P. Ducheyne, The effect of calcium phosphate ceramic composition and structure on in vitro behavior. II. Precipitation, J. Biomed. Mater. Res. 27 (1993) 35–44.
[17] S. Raynaud, E. Champion, D. Bernache-Assollant, P. Thomas, Calcium phosphate apatites with variable Ca/P atomic ratio I: synthesis, characterisation and thermal stability of powders, Biomaterials 23 (2002) 1065–1072.
[18] H.-S. Ryu, K.-S. Hong, J.-K. Lee, D.J. Kim, J.H. Lee, B.-S. Chang, D.-H. Lee, C.-K. Lee, S.-S. Chung, Magnesia-doped HA/beta-TCP ceramics and evaluation of their biocompatibility, Biomaterials 25 (2004) 393–401.
[19] C. Ergun, T.J. Webster, R. Bizios, R.H. Doremus, Hydroxylapatite with substituted magnesium, zinc, cadmium, and yttrium. I. Structure and microstructure, J. Biomed. Mater. Res. 59 (2002) 305–311.
[20] J. Marchi, A.C.S. Dantas, P. Greil, J.C. Bressiani, A.H.A. Bressiani, F.A. Muller, Influence of Mg-substitution on the physicochemical properties of calcium phosphate powders, Mater. Res. Bull. 42 (2007) 1040–1050.
[21] J. Ando, Tricalcium phosphate and its variations, Bull. Chem. Soc. Jpn. 31 (1958) 196–201.
[22] J. Ando, Phase diagrams of $Ca_3(PO_4)_2$-$Mg_3(PO_4)_2$ and $Ca_3(PO_4)_2$-$CaNaPO_4$ systems, Bull. Chem. Soc. Jpn. 31 (1958) 201–205.
[23] S. Kannan, J.M. Ventura, J.M.F. Ferreira, Aqueous precipitation method for the formation of Mg-stabilized β-tricalcium phosphate: an X-ray diffraction study, Ceram. Intern. 33 (2007) 637–641.
[24] L. Clausen, I. Fabricius, BET measurements: outgassing of minerals, J. Coll. Interf. Sci. 227 (2000) 7–15.
[25] F.B. Ayed, J. Bouaziz, K. Bouzouita, Calcination and sintering of fluorapatite under argon atmosphere, J. All. Comp. 322 (2001) 238–324.
[26] E. Landi, A. Tampieri, G. Celotti, S. Sprio, Densification behaviour and mechanisms of synthetic hydroxyapatites, J. Eur. Ceram. Soc. 20 (2000) 2377–2387.
[27] E. Bouyere, F. Gitzhofer, M.I. Boulos, Morphological study of hydroxyapatite nanocrystal suspension, J. Mater. Sci.: Mater. Med. 11 (2000) 523–531.
[28] A. Siddharthan, S.K. Seshadri, T.S. Sampath Kumar, Microwave accelerated synthesis of nanosized calcium deficient hydroxyapatite, J. Mater. Sci.: Mater. Med. 15 (2004) 1279–1284.
[29] R. Xin, Y. Leng, J. Chen, Q. Zhang, A comparative study of calcium phosphate formation on bioceramics in vitro and in vivo, Biomaterials 26 (2005) 6477–6486.
[30] Y.L. Zhang, M. Mizuno, M. Yanagisawa, H. Takadama, Bioactive behaviors of porous apatite- and wollastonite-containing glassceramic in two kinds of simulated body fluid, J. Mater. Res. 18 (2) (2003) 433–441.
[31] L.H. Guo, M. Huang, Y. Leng, J.E. Davies, X.D. Zhang, Structure and composition comparison of bone mineral and apatite layers formed in vitro, Key Eng. Mater. 192–195 (2001) 187–190.
[32] S.-H. Kwon, Y.-K. Jun, S.-H. Hong, H.-E. Kim, Synthesis and dissolution behaviour of β-TCP and HA/β-TCP composite powders, J. Eur. Ceram. Soc. 23 (2003) 1039–1045.
[33] M. Milosevski, J. Bossert, D. Milosevski, N. Gruevska, Preparation and properties of dense and porous calcium phosphate, Ceram. Intern. 25 (1999) 693–696.
[34] A. Bigi, G. Falini, E. Foresti, A. Ripamonti, Rietveld structure refinement of synthetic magnesium substituted β-tricalcium phosphate, Zeitschrift fur Kristallographic 211 (1996) 13–16.
[35] W.L. Suchanek, K. Byrappa, P. Shuk, R.E. Riman, V.F. Janas, K.S. TenHuisen, Preparation of magnesium-substituted hydroxyapatite powders by the mechanochemical–hydrothermal method, Biomaterials 25 (2004) 4647–4657.
[36] A. Bigi, G. Falini, E. Foresti, M. Gazzano, A. Ripamonti, N. Roveri, Magnesium influence on hydroxyapatite crystallization, J. Inorg. Biochem. 49 (1993) 69–78.
[37] A.C. Tas, F. Korkusuz, M. Timucin, N. Akkas, An investigation of the chemical synthesis and high-temperature sintering behaviour of calcium hydroxyapatite (HA) and tricalcium phosphate (TCP) bioceramics, J. Mater. Sci.: Mater. Med. 8 (1997) 91–96.
[38] S. Kannan, I.A.F. Lemos, J.H.G. Rocha, J.M.F. Ferreira, Synthesis and characterization of magnesium substituted biphasic mixtures of controlled hydroxyapatite/β-tricalcium phosphate ratios, J. Solid State Chem. 178 (2005) 3190–3196.
[39] R.Z. LeGeros, Calcium Phosphates in Oral Biology and Medicine, Karger AG, Basel, Switzerland, 1991.

[40] I.V. Fadeev, L.I. Shvorneva, S.M. Barinov, V.P. Orlovskii, Synthesis and structure of magnesium-substituted hydroxyapatite, Inorg. Mater. 39 (2003) 947–950.
[41] N. Jinlong, Z. Zhenxi, J. Dazong, Investigation of phase evolution during the thermochemical synthesis of tricalcium phosphate, J. Mater. Synth. Process. 9 (2002) 235–239.
[42] E.D. Eanes, I.H. Gillessen, A.S. Posner, Intermediate states in the precipitation of hydroxyapatite, Nature 208 (1965) 365–367.
[43] J.C. Heughebaert, Thesis, Institut National Polytechnique, Toulouse, 1977.
[44] R.S. Roth, J.R. Dennis, H.F. Mc Murdie, Phase diagrams for Ceramist, Edition K Reser, American Ceramic Society, Columbus, OH, 1964.
[45] L.W. Schroeder, B. Dickens, W.E. Brown, Crystallographic studies of the role of Mg as a stabilizing impurity in β-$Ca_3(PO_4)_2$ II. Refinement of Mg-containing β-$Ca_3(PO_4)_2$, J. Solid State Chem. 22 (1977) 253–262.
[46] A. Yasukawa, S. Ouchi, K. Kandori, T. Ishikawa, Preparation and characterization of magnesium–calcium hydroxyapatites, J. Mater. Chem. 6 (1996) 1401–1405.
[47] I. Mayer, R. Schlam, J.D.B. Featherstone, Magnesium-containing carbonate apatites, J. Inorg. Biochem. 66 (1997) 1–6.
[48] A. Rodrigues, A. Lebugle, Influence of ethanol in the precipitation medium on the composition, structure and reactivity of tricalcium phosphate, Colloids and Surfaces A: Physicochem. Eng. Aspects 145 (1998) 191–204.
[49] A. Mortier, J. Lemaitre, P.G. Rouxhet, Temperature-programmed characterization of synthetic calcium-deficient phosphate apatites, Thermochim. Acta 143 (1989) 265–282.
[50] A.Y. Malysheva, B.I. Beletskii, The state of water in tricalcium phosphate obtained by precipitation from a solution, Glass Ceram. 58 (2001) 3–4.
[51] E.R. Kreidler, F.A. Hummel, Phase equilibriums in the system calcium phosphate-zinc phosphate, Inorg. Chem. 6 (1967) 524–528.
[52] A. Tampieri, G. Celotti, F. Szontagh, E. Landi, Sintering and characterization of HA and TCP bioceramics with control of their strength and phase purity, J. Mater. Sci.: Mater. Med. 8 (1997) 29–37.
[53] S. Kannan, J.M.F. Ferreira, Synthesis and thermal stability of hydroxyapatite-tricalcium phosphate composite with cosubstituted sodium, magnesium and fluorine, Chem. Mater. 18 (2006) 198–203.
[54] T.R.N. Kutty, Assignments of some bands in the infrared spectrum of β-tricalcium phosphate, Indian J. Chem. 8 (1970) 655–657.
[55] Z. Zyman, M. Tkachenko, M. Epple, M. Polyakov, M. Naboka, Magnesium-substituted hydroxyapatite ceramics, Mat-wiss u Werkstofftech 37 (2006) 474–477.
[56] W.L. Suchanek, K. Byrappa, P. Shuk, R.E. Riman, V.F. Janas, K.S. TenHuisenb, Mechanochemical-hydrothermal synthesis of calcium phosphate powders with coupled magnesium and carbonate substitution, J. Solid State Chem. 177 (2004) 793–799.
[57] R.E. Mesmer, R.R. Irani, Changes in enthalpy during the heating of $CaHPO_4{\cdot}2H_2O$, J. Chem. Eng. Data 8 (1963) 530–532.
[58] J. Pena, M. Vallet-Regi, Hydroxyapatite, tricalcium phosphate and biphasic materials prepared by a liquid mix technique, J. Eur. Ceram. Soc. 23 (2003) 1687–1696.